J Mol Model (2012) 18:2727–2740
DOI 10.1007/s00894-011-1272-4

ORIGINAL PAPER

Quantum mechanical studies of lincosamides

Katarzyna Kulczycka-Mierzejewska · Joanna Trylska · Joanna Sadlej

Received: 16 June 2011 / Accepted: 5 October 2011 / Published online: 25 November 2011

Abstract Lincosamides are a class of antibiotics used both in clinical and veterinary practice for a wide range of pathogens. This group of drugs inhibits the activity of the bacterial ribosome by binding to the 23S RNA of the large ribosomal subunit and blocking protein synthesis. Currently, three X-ray structures of the ribosome in complex with clindamycin are available in the Protein Data Bank, which reveal that there are two distinct conformations of the pyrrolidinyl propyl group of the bound clindamycin. In this work, we used quantum mechanical methods to investigate the probable conformations of clindamycin in order to explain the two binding modes in the ribosomal 23S RNA. We studied three lincosamide antibiotics: clindamycin, lincomycin, and pirlimycin at the B3LYP level with the 6-31G** basis set. The focus of our work was to connect the conformational landscape and electron densities of the two clindamycin conformers found experimentally with their physicochemical properties. For both functional conformers, we applied natural bond orbital (NBO) analysis and the atoms in molecules (AIM) theory, and calculated the NMR parameters. Based on the results obtained, we were able to show that the structure with the intramolecular hydrogen bond C=O···H–O is the most stable conformer of clindamycin. The charge transfer between the pyrrolidine-derivative ring and the six-atom sugar (methylthiolincosamide), which are linked via an amide bond, was found to be the dominant factor influencing the high stability of this conformer.

Keywords Ribosome · Bacterial translation · Lincosamides · Ab initio calculations · Clindamycin

K. Kulczycka-Mierzejewska · J. Trylska
Interdisciplinary Centre for Mathematical and Computational Modelling, University of Warsaw,
Pawinskiego 5A,
02-106 Warsaw, Poland

K. Kulczycka-Mierzejewska
College of Inter-faculty Individual Studies in Mathematics and Natural Science, University of Warsaw,
Zwirki i Wigury 93,
02-089 Warsaw, Poland

J. Sadlej (✉)
Faculty of Chemistry, University of Warsaw,
Pasteura 1,
02-093 Warsaw, Poland
e-mail: sadlej@chem.uw.edu.pl

Introduction

The three compounds lincomycin (a natural antibiotic produced by *Streptomyces lincolnensis* and discovered in 1961), clindamycin, and pirlimycin (two semi-synthetic derivatives of lincomycin) comprise a group of clinically important antibiotics known as lincosamides.

The structure of lincomycin (Fig. 1a) can be divided into two parts, a pyrrolidine derivative and a six-atom sugar ring (methylthiolincosamide), which are linked via an amide bond in the central part of the molecule. Clindamycin (Fig. 1b) is obtained by 7(*S*)-chloro-substitution of the 7(*R*)-hydroxyl group of lincomycin, and pirlimycin (Fig. 1c) is obtained by trimming the propyl group of clindamycin to get an ethyl group. These compounds are soluble in water and chemically stable both in the dry state and in solution.

Lincosamides block bacterial protein synthesis, which takes place on the ribosomes. Ribosomes are organelles that are composed of ribosomal RNAs (rRNA; ca. 65% by mass) and proteins (ca. 35%) [1]. The bacterial 70S ribosome can be separated into two subunits: large (50S) and small (30S), named after their sedimentation coeffi-

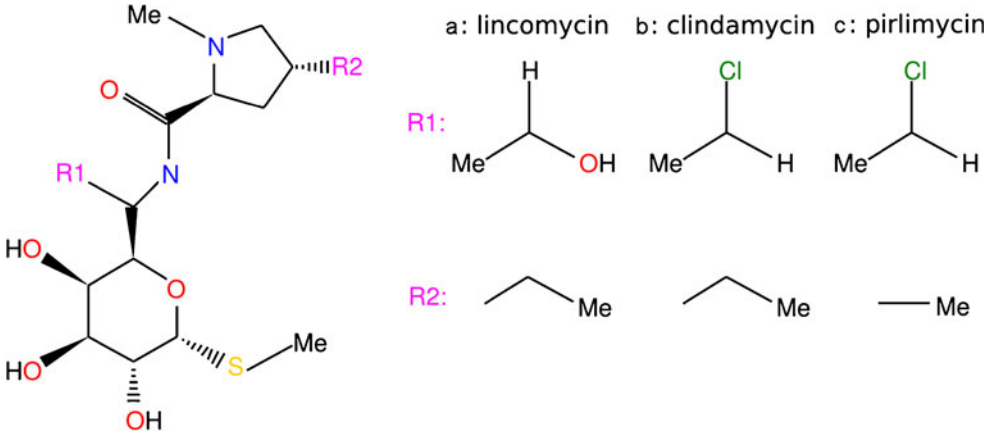

Fig. 1 Chemical structures of lincosamides: lincomycin (natural antibiotic, *a*) and its semi-synthetic derivatives clindamycin (*b*) and pirlimycin (*c*)

cients. The small subunit of prokaryotic ribosomes consists of 21 proteins and one 16S RNA chain, while the large subunit contains over 30 proteins and two RNA chains (23S RNA and 5S RNA). Lincosamides bind to the 23S RNA (interacting with the A- and P-tRNA binding sites) of the 50S ribosomal subunit and inhibit the peptidyltransferase reaction, i.e., peptide bond formation [2]. Therefore, they typically have a bacteriostatic mode of action.

The main spectrum of action of lincosamides includes bacteria associated with skin infections, and lincosamides are first-choice antibiotics used in veterinary dermatology. However, although they do have adverse effects, such as nausea, rash, or abdominal pain, lincomycin and clindamycin are also effectively used in human medicine [3]. Clindamycin shows stronger antibacterial activity than lincomycin. Lincosamides are effective against Gram-positive bacteria, such as *Staphylococcus*, *Streptococcus*, most anaerobic bacteria (e.g., *Bacteroides fragilis*), and some protozoa. In the latter case, they can serve as an antimalarial drug. Gram-negative bacteria are, in general, resistant to lincosamides, with one important exception: *Capnocytophaga canimorsus* [4].

Lincosamides exhibit excellent pharmacokinetic properties; they are well absorbed orally and can penetrate well into infected skin. Also, the minimum inhibitory concentration (MIC_{90}, the minimum concentration needed to inhibit growth overnight in 90% of organisms) of clindamycin towards *Streptococcus pyogenes* is over 120 times lower than that of tetracycline [5]. Unfortunately, extensive use of these antibiotics has led to increased resistance in many strains of bacteria, which have been developing various mechanisms to counter these drugs. One known mechanism is structural modification of the drug's target (ribosome) through the methylation of 23S RNA (e.g., base no. 2058 [6]) and/or mutations (e.g., of bases G2057, A2058, A2059, C2452, and C2611 [7]). Other mechanisms of resistance are active efflux of the drug across the cell surface, or its enzymatic deactivation [8]. Bacterial resistance together with side effects are the most important reasons for improving known lincosamides and designing modified compounds.

The conformational properties of free clindamycin and lincomycin have been studied using X-ray techniques [9, 10] as well as ^{1}H and ^{13}C NMR spectroscopy and molecular dynamics [11]. However, Verdier et al. [11] also investigated lincosamide–ribosome interactions by two-dimensional transferred nuclear Overhauser effect spectroscopy (TRNOESY), and showed that the conformation of the lincosamide plays a crucial role in its binding to the ribosome. Ravikumar et al. [9] reported the crystal structures of clindamycin hydrochloride monohydrate and its ethanol solvate. They found that the free conformers of clindamycin and LinB (lincosamide nucleotidyltransferase) enzyme-bound clindamycin are similar [12]. Rajeswaran et al. [10] solved the X-ray structure of lincomycin hydrochloride and found that intra- and intermolecular hydrogen bonds stabilize the structure of the drug. On the other hand, pirlimycin has not been subjected to extensive theoretical studies.

There are four crystallographically resolved structures of clindamycin bound to a target: three in complex with the ribosome [13–15], and one with the LinB molecule [12], the bacterial enzyme responsible for the inactivation of lincosamides by nucleotidylation. Their crystal structures as well as the structure of the native ribosome [16] are available through the Protein Data Bank (PDB). These crystallographic data form the basis for our theoretical studies of chemical and physical properties of lincosamides. Two out of the three conformers of clindamycin, when bound to the ribosome, show significant differences between antibiotic conformations: in two structures, the pyrrolidynyl propyl group is rotated by 180° relative to the other conformer. Clindamycin shows intramolecular hydrogen bonds that stabilize the respective conformations.

Theoretical calculations provide a complementary way to study molecular systems containing an intramolecular hydrogen bond (IHB). Although the accuracy of ab initio

calculations is still below the state-of-art accuracy of experimental spectroscopic data, these calculations provide information about the shape of the potential energy surface (PES) without the need for any initial assumptions. Characterizing the conformational changes and their possible effects on the encounter with and binding to the ribosome are important aspects of understanding the mechanism of action of lincosamides. To the best of our knowledge, no systematic and accurate study of the conformational behavior of clindamycin in the gas phase and in solution has been reported. The aim of the work described in the present paper was to clarify the role of intramolecular hydrogen bonds in clindamycin using quantum chemical calculations. These ab initio calculations consist of the following steps: the choosing the model structures, geometry optimization, natural bond orbital analysis (NBO), atoms in molecules analysis (AIM), and spectroscopic NMR parameter calculations, which are currently among the most popular methods used for conformational analysis.

The methods applied in the calculations are described in the first section of the paper. We then characterize the conformations and molecular properties, focusing on the intramolecular hydrogen bonds. The paper concludes with a summary.

Computational details

The first step was to prepare models of the antibiotics. Four structures of clindamycin are available in the Protein Data Bank [17] (as of May 2011). Three of these structures are in complex with the bacterial ribosome [13–15], while one is in complex with LinB [12]. The two ribosome-complexed structures show similar clindamycin conformers, and in one the pyrrolidynyl propyl group is rotated by 180°. In this work, we used two significantly different conformers of clindamycin, which were taken from ribosome–clindamycin complexes of *Deinococcus radiodurans* [13] (PDB code 1JZX) and *Haloarcula marismortui* [14] (PDB code 1YJN). The experimental structures of lincomycin and pirlimycin are not available. Therefore, based on the known X-ray structures of clindamycin (Fig. 2), we built two analogical conformers of both lincosamides.

The second step involved optimizing the geometries of all of the antibiotic models constructed, using density functional theory (DFT) at the B3LYP level [18, 19] with the 6-31G** basis set and a redundant coordinate algorithm [20].

We considered two cases for the optimization procedure. In the first case, we optimized the investigated molecules

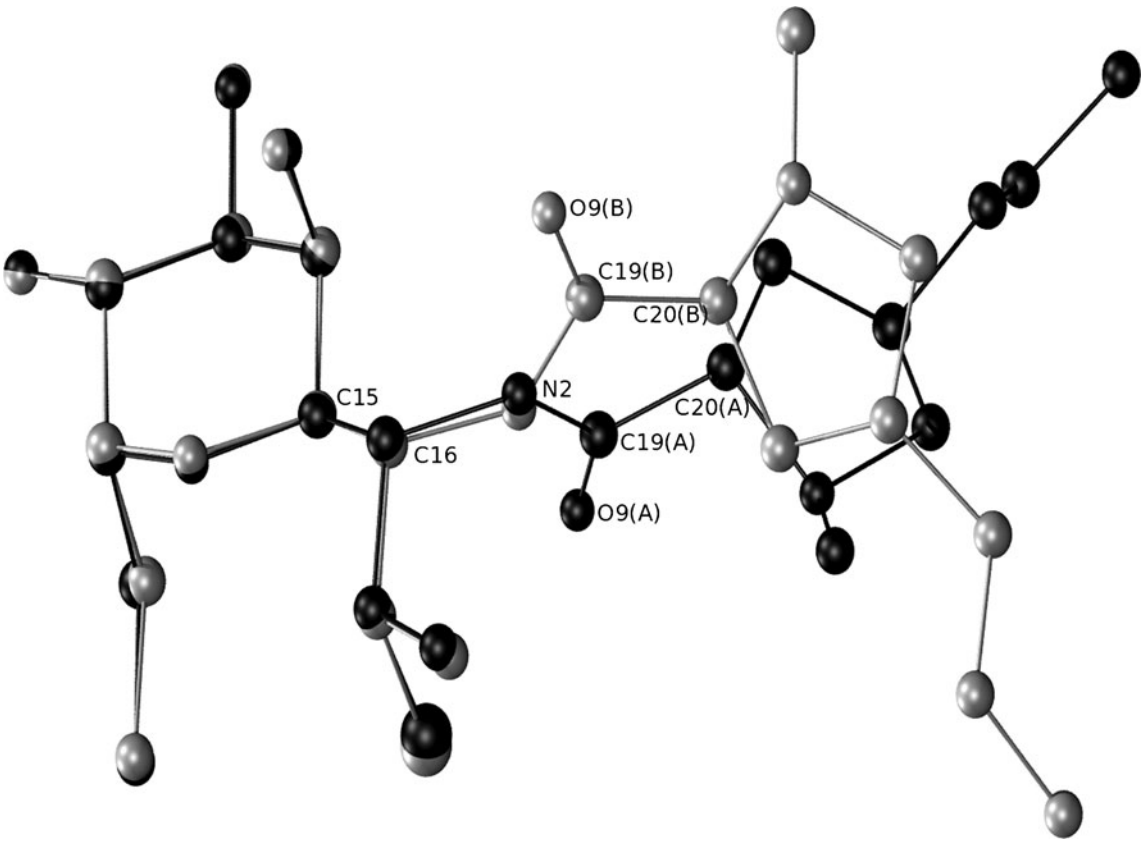

Fig. 2 Ball and stick representation showing the superposition of two clindamycin conformers when bound to the ribosome. *Black* conformer A, *gray* conformer B (only heavy atoms are shown for clarity)

without any constraints. In the second case, the two dihedral angles *d*(C15–C16–N2–C19) and *d*(C16–N2–C19–C20), which are significantly different in both experimentally known conformers (A and B; see Fig. 2), were kept constant in the optimization procedure to differentiate between the two conformers. The values of the dihedral angles *d*(C15–C16–N2–C19) and *d*(C16–N2–C19–C20) for conformer A were set to −47° and −180°, while they were set to 119° and 178°, respectively, for conformer B, in accordance with known experimental results. Thus, we obtained two conformations that are minima on the PES. The corresponding frequency calculations were carried out at the same level in order to confirm the nature of the stationary points. No imaginary frequencies were observed, which means that the structures of the antibiotics are true minima. These structures, which we called "exp-opt," were used during AIM, NBO, and NMR calculations (see below).

In a third step, in order to explore the conformational landscape of the molecules, we performed a potential energy surface scan along the torsional coordinates mentioned above in a relaxed manner (i.e., all other geometrical parameters were optimized at each point) for both conformers. The scan was calculated using the B3LYP/6-31G** method.

Most spectroscopic measurements are performed on liquid samples. To describe the environment of the antibiotic, either the continuum solvation model or an atomic representation of the solvent can be used. Therefore, as a fourth step, in order to study the solvent effect, optimization and frequency calculations were also performed at the B3LYP/6-31G** level of theory in combination with the polarizable continuum solvent model based on the integral equation formalism (IEF-PCM) [21]. In this model, the solvent is described by a dielectric constant, which was set to 80 in our work. The second model that was used to describe the environment of the antibiotic, and mimics the surroundings of the antibiotic in the ribosomal RNA, was the model with point ions placed around the antibiotic [22, 23]. The positions of these point charges were obtained from the X-ray structures of the ribosome–clindamycin complexes [13, 14]. The coordinates of residues within 10 Å of each clindamycin atom were considered, and partial charges were assigned based on the G43b1 GROMOS96 force field [24].

In this way, we studied the effect of the charged ribosome environment on the conformations of the lincosamides.

Next, in order to gain a deeper insight into the nature of the conformational changes, NBO and AIM electron density analyses were applied for the two analyzed conformers of clindamycin. The bond critical points (BCPs) were characterized in terms of electron density and their Laplacian values. These gas-phase calculations were performed at the B3LYP/6-31G** level.

NMR spectroscopy is one of the techniques used to investigate molecular structures and interactions. In the last

Table 1 Total energies (E_0, in au), zero-point energies (ZPE, in kcal/mol), and relative Gibbs free energies at 298.15 K (ΔG, in kcal/mol). Top: values for the fully optimized A and B conformers of clindamycin, lincomycin, and pirlimycin in vacuum. Bottom: values for the A and B conformers of clindamycin, lincomycin, and pirlimycin (optimized using a redundant coordinate algorithm in vacuum) in the PCM model of solvent and in the point ions. Two dihedrals were kept constant, *d*(C15–C16–N2–C19)=−47.0 and *d*(C16–N2–C19–C20) =−180.0 for conformer A, and *d*(C15–C16–N2–C19)=119.0 and *d*(C16–N2–C19–C20)=178.0 for conformer B. All calculations were performed at the B3LYP/6-31G** level

	Clindamycin		Lincomycin		Pirlimycin	
	A	B	A	B	A	B
Fully optimized structures						
E_0	−2049.831737	−2049.846556	−1665.458409	−1665.463660	−2010.515225	−2010.54063381
ZPE	323.26	323.66	332.14	332.40	305.59	305.85
ΔG	8.20	0.0	2.41	0.0	15.69	0.0
Structures with frozen dihedrals C15–C16–N2–C19 and C16–N2–C19–C20						
E_0	−2049.831704	−2049.844535	−1665.456720	−1665.455960	−2010.514391	−2010.455988
ZPE	323.29	323.53	332.19	331.99	305.35	305.37
ΔG	8.05	0.0	0.23	0.0	5.32	0.0
E_0^{PCM}	−2049.796886	−2049.804378	−1665.418265	−1665.419456	−2010.441623	−2010.460224
ZPE^{PCM}	323.87	324.10	332.77	332.56	305.92	305.94
ΔG^{PCM}	6.58	0.0	0.43	0.0	5.40	0.0
E_0^{ions}	−2048.43909665	−2048.44804200	−1664.05485157	−1664.05656314	−2009.11644087	−2009.12370514
ZPE^{ions}	329.99	329.71	339.94	339.56	312.95	312.74
ΔG^{ions}	5.55	0.0	1.07	0.0	3.86	0.0

part of our work, we calculated the NMR chemical shifts and spin–spin coupling constants for the gas-phase optimized geometries at the B3LYP/6-31G** level. Shielding constants were calculated using the B3LYP/aug-pcS-1 [25] method and the GIAO routine [26–30]. The chemical shifts of the *i*-th nuclei were calculated as $\delta(i) = \sigma_i(X) - \sigma_i(C)$, where σ_i(C) and σ_i(X) are the isotropic parts of the shielding tensors of the *i*-th nuclei in clindamycin and the *i*-th nuclei in the reference X molecule, respectively. The spin–spin coupling constants were calculated at the B3LYP/aug-pcJ-0 [31, 32] level. The nonstandard basis sets were taken from the EMSL Basis Set Library [33, 34].

All of the calculations were carried out using the GAUSSIAN03 and GAUSSIAN09 software packages [35]. The NBO calculations were performed with the NBO 5.0 program [36], while AIM calculations were performed using AIM2000 [37]. Data were analyzed using Gabedit [38], and the visualizations were carried out with VMD [39] and XDrawChem.

Results and discussion

Conformational analysis

The energies, the zero-point vibrational energies (ZPE), and the Gibbs free energy (ΔG) values based on the harmonic field relative to the most stable one at 298.15 K calculated in the gas phase, taking solvent effects into account, are depicted in Table 1. The selected geometric parameters obtained from gas-phase calculations for both conformers of clindamycin, lincomycin, and pirlimycin in their bound modes are given in Table 2. Their structures and atom numbering schemes are presented in Fig. 3.

Table 2 Selected geometric parameters (in Å and degrees) for the "exp-opt" structures of both conformers (A and B) of clindamycin, lincomycin, and pirlimycin calculated at the B3LYP/6-31G** level in vacuum

	Clindamycin		Lincomycin		Pirlimycin	
	A	B	A	B	A	B
r(S1–C11)	1.855	1.857	1.850	1.852	1.854	1.857
r(C12–O4)	1.422	1.415	1.421	1.413	1.422	1.414
r(C12–C13)	1.526	1.536	1.421	1.537	1.527	1.536
r(C13–O5)	1.426	1.412	1.425	1.412	1.426	1.412
r(C15–O7)	1.443	1.432	1.451	1.438	1.441	1.430
r(O7–C11)	1.412	1.416	1.418	1.820	1.413	1.415
r(C15–C16)	1.543	1.545	1.549	1.544	1.542	1.538
r(C16–C17)	1.543	1.536	1.558	1.555	1.542	1.538
r(C17–O8)	–	–	1.427	1.419	–	–
r(C17–Cl28)	1.833	1.852	–	–	1.832	1.852
r(C17–C18)	1.523	1.521	1.525	1.526	1.524	1.520
r(C16–N2)	1.462	1.457	1.466	1.462	1.462	1.456
r(N2–C19)	1.371	1.362	1.365	1.370	1.372	1.369
r(C19–O9)	1.223	1.232	1.229	1.230	1.222	1.231
r(C19–C20)	1.542	1.533	1.542	1.537	1.541	1.536
r(C20–N3)	1.462	1.452	1.482	1.457	1.460	1.458
r(N3–C21)	1.450	1.451	1.450	1.454	1.450	1.454
r(N3–C22)	1.459	1.459	1.465	1.459	1.458	1.459
r(C22–C23)	1.537	1.537	1.531	1.533	1.538	1.532
r(C23–C24)	1.557	1.557	1.542	1.552	1.559	1.551
r(C24–C20)	1.548	1.558	1.542	1.561	1.548	1.561
a(C20–C19–N2)	113.8	114.5	–	–	–	–
a(C19–N2–C16)	128.6	124.2	–	–	–	–
a(N2–C16–C15)	113.8	112.2	–	–	–	–
a(N2–C16–C17)	113.0	110.8	–	–	–	–
a(C16–C17–C18)	113.2	113.9	–	–	–	–
a(C16–C15–C14)	111.9	123.0	–	–	–	–
a(O9–C19–N2)	124.4	123.0	–	–	–	–
d(C15–C16–N2–C19)	−47.0	119.0	−47.0	119.0	−47.0	119.0
d(C16–N2–C19–C20)	−180.0	178.0	−180.0	178.0	−180.0	178.0

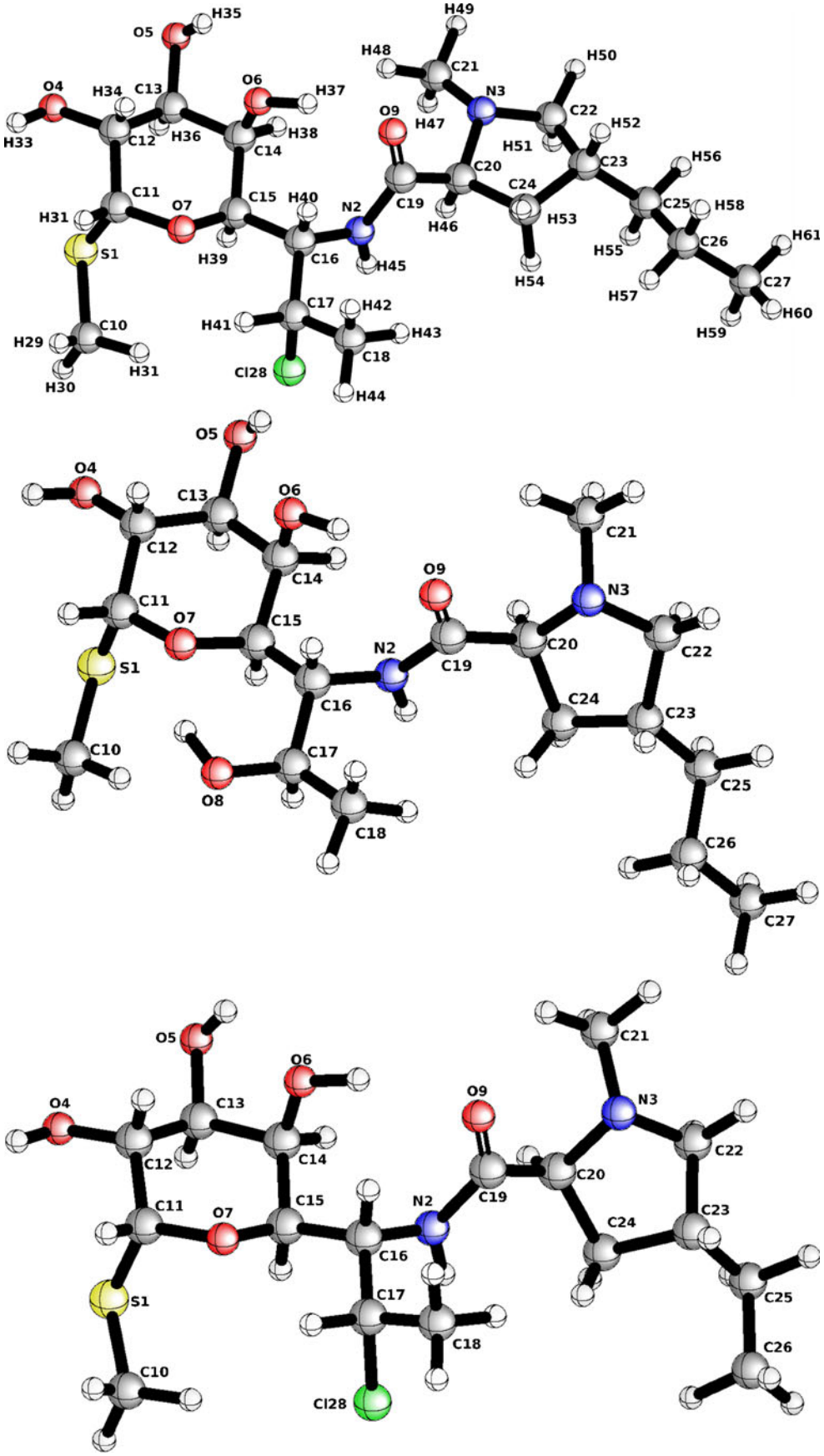

Fig. 3 Ball and stick models of the studied molecules and their atom numbering schemes. *Top*: clindamycin, *middle*: lincomycin, *bottom*: pirlimycin

A number of factors influence the structure and stability of the conformers of clindamycin. Our results show that the most important is the energy profit from the formation of the IHB. The presence of hydrogen-bond donors (O–H, N–H, C–H) and hydrogen-bond acceptors (C=O, Cl) allows for a range of hydrogen-bond combinations and a number of stable forms [40, 41]. Let us now concentrate on the C19–O9⋯H37–O6 IHB. Because of the internal hydrogen bonds, one conformer is stabilized to a greater extent than the others. First and foremost, at the B3LYP/6-31G** level, the most stable clindamycin B conformer is more energetically favored than the next most stable by as much as 8.0 kcal/mol. The energetic picture significantly changes for lincomycin and pirlimycin. In the case of lincomycin, no single conformer is favored at 298.15 K, while the A conformer of pirlimycin is more stable than B according to the three models used: vacuum, PCM, and point ions. The clindamycin B conformer in vacuum displays both the longest O6–H37 bond (0.980 Å) and the shortest IHB distance, *r*(C19–O9⋯H37–O6)=1.819Å. The *r*(C19–O9⋯H39–C15) IHB distance in the less stable A conformer is 2.370 Å, and *r*(C15–H39)=0.970 Å is the most important component of the

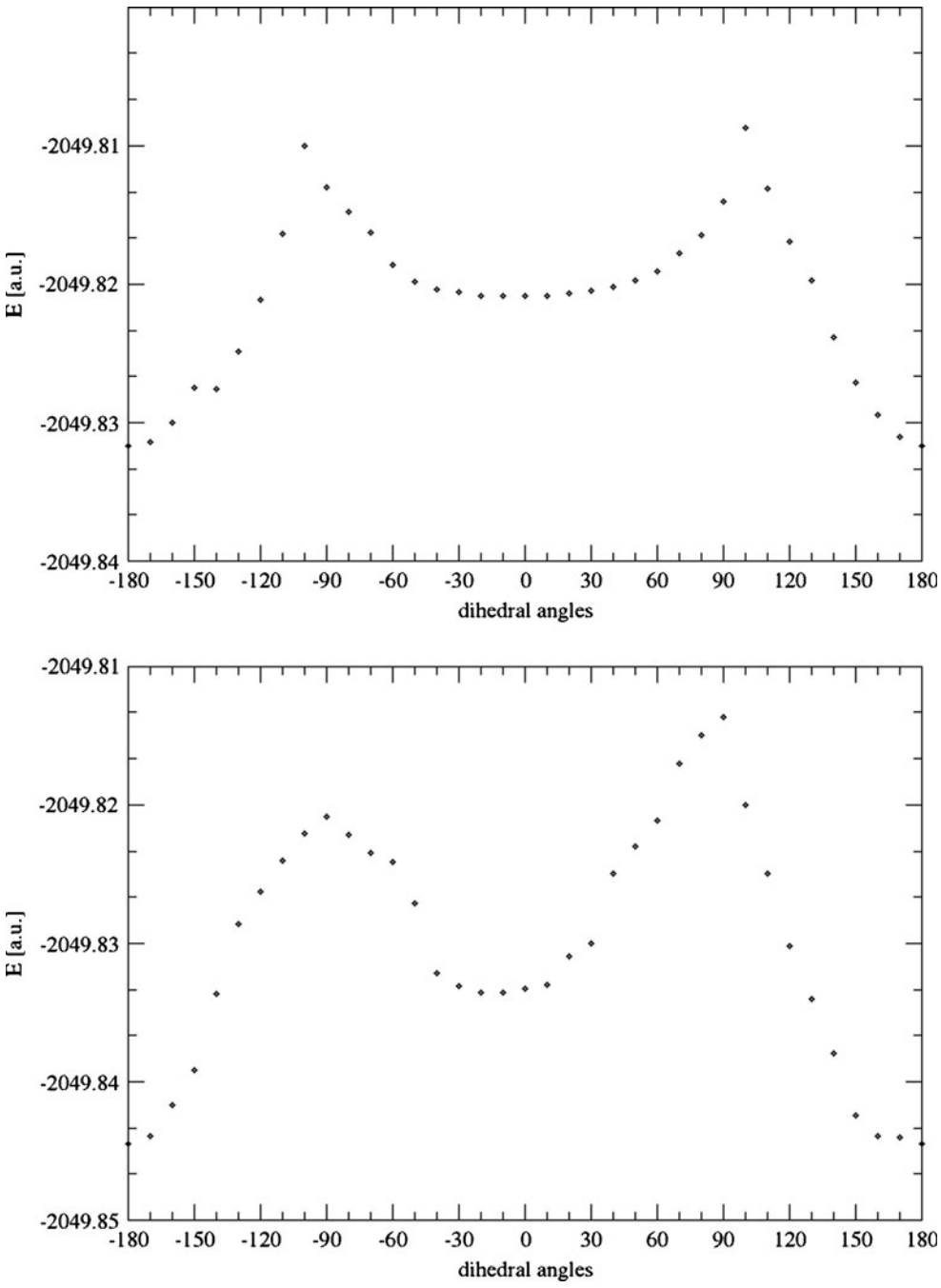

Fig. 4 Changes in the energy (in au) of the C15–C16–N2–C19 dihedral angle in both clindamycin conformers, A (*top*) and B (*bottom*) in vacuum; calculations were performed with the B3LYP/6-31G** method

Table 3 Selected second-order perturbation energy (ΔE^2, in kcal/mol) between donor and acceptor orbitals and charge transfer ($\Delta q_{i,j}$, in au) in the A (top) and B (bottom) conformers of clindamycin. Calculations were performed for "exp-opt" structures at the B3LYP/6-31G** level in vacuum

$NBO_{donor\ (i)}$	$NBO_{acceptor\ (j)}$	ΔE^2 (kcal/mol)	$\Delta q_{i,j}$ (au)
A			
LPN2	σ^*C19–O9	57.27	0.118
LPN3	σ^*C22–H45	7.89	0.068
LPN3	σ^*C20–H50	7.73	0.066
LPN3	σ^*C21–H48	8.31	0.069
LPO4	σ^*C12–C11	8.52	0.068
LPO6	σ^*C14–C13	4.32	0.048
LPO6	σ^*C14–H37	7.11	0.066
LPO9	RY*C19	16.51	0.142
LPO9	σ^*C20–C19	20.86	0.103
LPO9	σ^*C19–N2	26.11	0.124
LPO9	σ^*C15–H39	0.93	0.024
B			
LPN2	σ^*C19–O9	60.17	0.119
LPO5	σ^*C13–C12	9.21	0.069
LPO6	σ^*C15–C14	9.07	0.070
LPO9	RY*C19	14.25	0.132
LPO9	σ^*C20–C19	21.04	0.106
LPO9	σ^*C19–N2	20.38	0.112
LPO9	σ^*O6–H37	8.60	0.074

conformer's stability. The differences in the geometries of the two clindamycin conformers are related almost exclusively to the IHBs in the central part of the molecule. For the most stable conformer, B, an eight-atom ring is formed, whereas a six-atom ring is found in the A conformer.

Potential energy scans for internal rotation around the C–N single bond were obtained by allowing the C15–C16–N2–C19 dihedral angle to vary from 0 to 180° for clindamycin in vacuum and an aqueous PCM phase. The values of the starting dihedrals were different in the A and B conformers, as shown in Fig. 2. Full geometry optimizations at a fixed dihedral angle with an increment of 10° were carried out. The graphs of potential energy as a function of the dihedral angle for gas-phase calculations are shown in Fig. 4. To estimate the influence of its surroundings on the conformation of clindamycin, both conformers that are stable in the gas phase were analyzed using the IEF-PCM/B3LYP/6-31G** method. Table 1 confirms that solvation has a relatively small effect on the energy difference between conformers. The B conformer of clindamycin is favored over the A conformer by 6.6 and 5.6 kcal/mol according to the PCM and point-ion models, respectively.

Natural bond analysis

In general, the differences in the conformations of the two models of clindamycin can be understood qualitatively in terms of changes in bond lengths, angles, and the electron density distribution over the whole structure. Natural population analysis [42] is recognized as a reliable tool to rationalize different trends observed in molecules containing IHB. In this section, we will discuss the results of NBO calculations.

Analysis of the Mülliken charges for the heavy atoms (data not shown) suggests relationships between the charges and geometrical parameters of the two conformers. The ring with IHB in the B conformer of clindamycin consists of one nitrogen (N2) atom with a charge of −0.53 au, two oxygen atoms (O9 and O6) with charges of −0.54 au and −0.59 au, and carbon atoms with charges ranging from 0.60 au to 0.02 au. In the A conformer of clindamycin, the negative charges of both oxygens are slightly decreased, while both carbon atoms become more positive (0.61 au, 0.07 au). Such a decrease in negative charge with the changes in

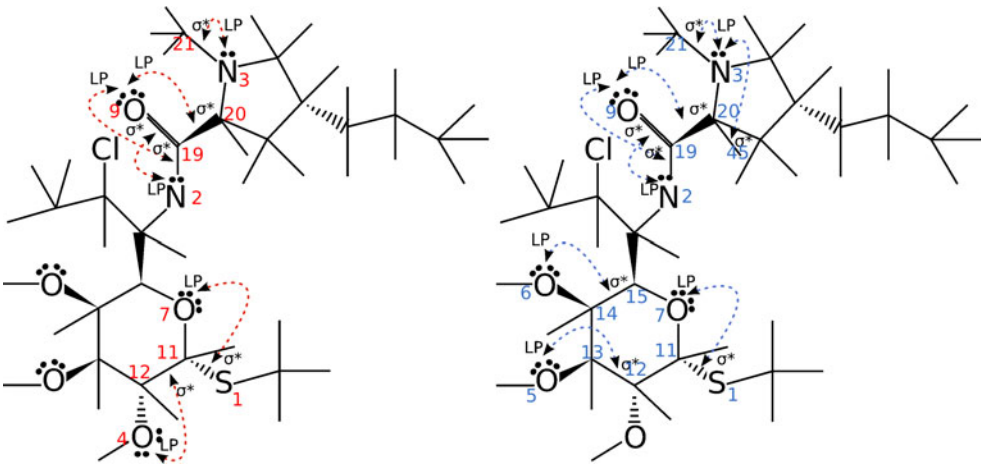

Fig. 5 Representations of hyperconjugative intramolecular interactions, based on the NBO analysis of both clindamycin "exp-opt" conformers: *red dashed line* for A (*left*), *blue dashed line* for B (*right*); B3LYP/6-31G** in vacuum

torsional angles that occur when moving from the B to the A conformer is related to the fractional transfer of the charge to electronegative oxygen atoms in the B conformer of clindamycin.

The second-order perturbation energy (ΔE^2) due to the interaction energy between the donor and acceptor orbitals in the central part of the molecule together with the charge transfer (CT) between two moieties of the molecule are

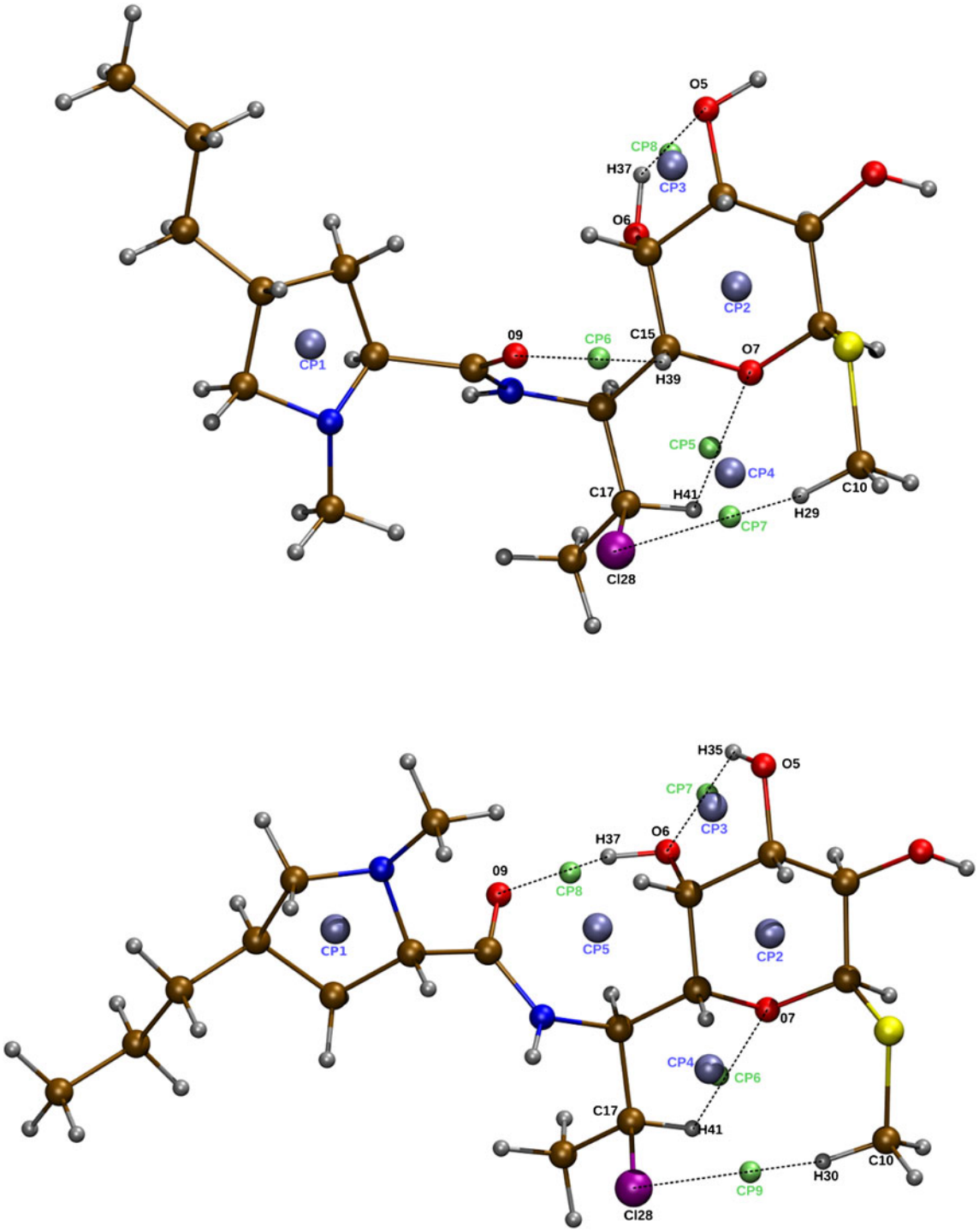

Fig. 6 Molecular graphs of both "exp-opt" conformers of clindamycin (*top*: A, *bottom*: B) based on critical points obtained from the AIM analysis. The *brown*, *red*, *blue*, *yellow*, *purple*, and *silver beads* represent C, O, N, S, Cl, and H atoms, respectively. The *light violet* and *light green beads* represent the (3, +1) and (3, −1) critical points, respectively. The H-bonds [paths connecting the (3, −1) critical points] are marked with *dashed lines*

presented in Table 3. The selected orbital interactions (with a stabilizing effect of over 8 kcal/mol) are presented in Fig. 5 for both clindamycin conformers.

Considering that the charge transfer accompanies the formation of IHB in the NBO model, the donor–acceptor interaction energies ΔE^2 can be taken as a measure of the strength of the intramolecular interaction. In the case of the central H45–N2–C19–O9 group, the CT from the lone pair orbital on N2 is mainly directed to the antibonding $\sigma^*_{C19–O9}$ orbital (0.118 in the A conformer and 0.119 au in the B conformer). Other important charge-transfer stabilizations are observed between the lone pair orbital of O9 and the antibonding $\sigma^*_{C20–C19}$ orbital (0.103 for the A conformer and 0.106 au for the B conformer), as well as between the lone pair of the O9 orbital and the antibonding $\sigma^*_{C19–N2}$ orbital (0.124 for the A conformer and 0.112 au for the B conformer). Additionally, for the A conformer, we found quite a strong interaction between the lone pair orbital on O4 and the antibonding $\sigma^*_{C12–C11}$ orbital (0.068 au). Similar interactions were also seen for the B conformer. The lone pair orbital on O6 interacts with the antibonding $\sigma^*_{C15–C14}$ one (0.070 au), and the lone pair orbital on O5 with the antibonding orbital $\sigma^*_{C13–C12}$ (0.069 au). On the other hand, the CT that occurs from the lone pair orbital on O9 through the IHB to the antibonding $\sigma^*_{H39–C15}$ orbital (0.024 au) for the A conformer is lower than that for the $\sigma^*_{H37–O6}$ orbital of the B conformer (0.074 au). To summarize, NBO analysis indicates that the occupancy of the antibonding $\sigma^*_{C15–H39}$ orbital in the A conformer or the $\sigma^*_{O6–H37}$ orbital of the eight-member moiety in the B conformer should be an overall indicator of conformational stability. Therefore, the charge transfer between the pyrrolidine-derivative ring and the six-atom sugar (methylthiolincosamide), which are linked via an amide bond, is the dominant factor in the greater stability of the B conformer.

Atoms in Molecules analysis

The absence or presence of many types of hydrogen bonds can influence the energy properties of molecular conformers. In many cases, the Atoms in Molecules (AIM) method is a practical tool for understanding the properties of hydrogen bonds. It identifies a unique line of communication between two nuclei, and provides a point describing the nature of this interaction. Topological analysis of the electron density distribution provides evidence for bonding interactions through the discovery of a (3, −1) critical point (ρ_{BCP}), which is a key topological descriptor of internuclear interactions, while the Laplacian of the electron density values at the critical point $\nabla^2\rho_{BCP}$ is another sensitive measure of the

Table 4 The lengths of H-bonds and the electron density and Laplacian values for selected critical points of the A (top) and B (bottom) clindamycin "exp-opt" conformers optimized at the B3LYP/6-31G** level in vacuum

Critical point no.	Atom numbers and names	d_{HB}	ρ_{CP}	$\nabla^2\rho_{CP}$
A				
Rings				
CP1	N3–C20–C22–C23–C24	–	0.0381	−0.0689
CP2	O7–C11–C12–C13–C14–C15	–	0.0185	−0.0301
CP3	O5–H37–O6–C13–C14	–	0.0191	−0.0250
CP4	O7–C15–C16–C17–H41	–	0.0026	−0.0027
H-bonds				
CP5	C15–O7···H41–C17	2.322	0.0155	−0.0164
CP6	C19–O9···H39–C15	2.370	0.0146	−0.0131
CP7	C17–Cl28···H29–C10	2.982	0.0055	−0.0044
CP8	C13–O5···H37–O6	2.147	0.0195	−0.0194
B				
Rings				
CP1	N3–C20–C22–C23–C24	–	0.0380	−0.0678
CP2	O7–C11–C12–C13–C14–C15	–	0.0027	−0.0023
CP3	O5–H35–O6–C14–C13	–	0.0271	−0.0285
CP4	O7–C15–C16–C17–H41	–	0.0212	−0.0027
CP5	O6–H37–O9–C19–N2–C16–C15–C14	–	0.0091	−0.0105
H-bonds				
CP6	C15–O7···H41–C17	2.320	0.0154	−0.0162
CP7	C14–O6···H35–O5	2.102	0.0222	−0.0203
CP8	C19–O9···H37–O6	1.819	0.0340	−0.0248
CP9	C17–Cl28···H30–C10	3.000	0.0053	−0.0043

properties of a classical bond. It should be noted that there is some controversy regarding the use of AIM as a diagnostic tool for bonding interactions [43]. However, typical intermolecular as well as intramolecular H-bonds can be categorized properly, as has been proven in the literature [44, 45].

The Popelier criteria [44, 46] for hydrogen-bond formation include the requirement that ρ_{BCP} is in the range 0.002–0.040 au, and the need for the value of the Laplacian at the hydrogen-bond critical point $\nabla^2\rho_{BCP}$ to be between 0.02 and 0.15 au. It is not, however, always necessary to fulfill these criteria [47]. A negative Laplacian reveals excess potential energy at the BCP, meaning that the electronic charge is concentrated into a bond. A positive $\nabla^2\rho_{BCP}$ reflects an excess of kinetic energy in a bond, indicating a local depletion of the electron density along a bond path. In other words, generally, the Laplacian of ρ is positive when ρ is locally reduced, and negative if it is locally concentrated.

According to criteria elaborated by the AIM theory, we found two types of intramolecular H-bonds in clindamycin: typical hydrogen bonds of type CH···OC in the A

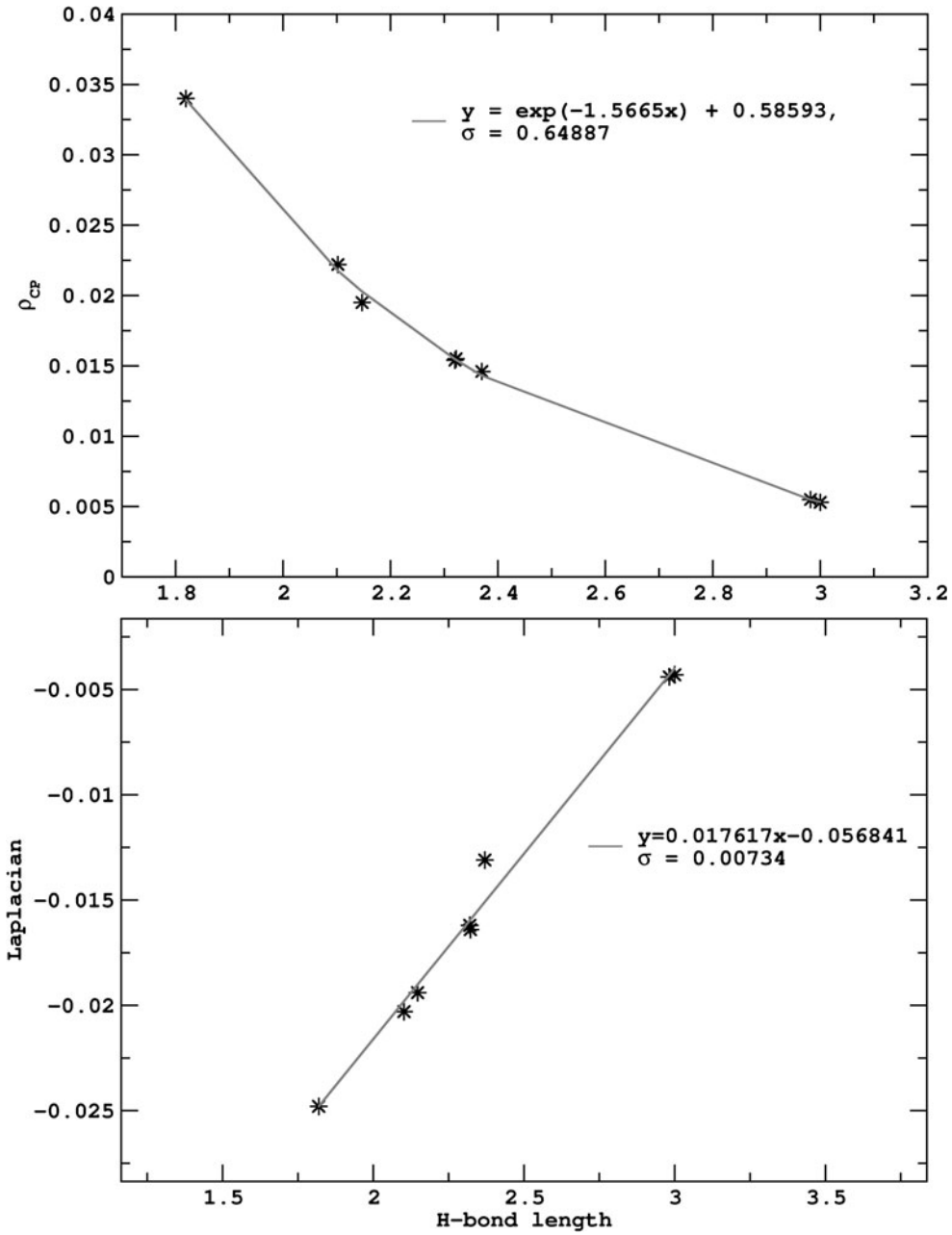

Fig. 7 The electron density ρ_{CP} (*top*) and the Laplacian $\nabla^2\rho_{CP}$ (*bottom*) as functions of intramolecular hydrogen-bond length in both conformers of clindamycin

conformer and OH···O=C in the B conformer, and unconventional H-bonds of type OH···X (X=O, Cl) in both conformers (Fig. 6). The numerical values for the electron density (ρ_{BCP}) and Laplacian ($\nabla^2\rho_{BCP}$) are presented in Table 4. Figure 7 shows plots of ρ_{BCP} (top) and $\nabla^2\rho_{BCP}$ (bottom) versus the length of the hydrogen bond $r_{O...H}$. The general shape of the ρ_{BCP} curve is that of an exponential decay, as expected (see Fig. 7). The linear correlation between $\nabla^2\rho_{BCP}$ and $r_{O...H}$ illustrates (Fig. 7) that, in accordance with chemical intuition, $\rho_{O...H}$ is increased in an IHB.

The electron density at the critical points is equal to 0.034 au for the B conformer (BCP8) and 0.014 au for the A conformer (BCP6), which is in line with the most stable B structure. $\nabla^2\rho_{BCP}$, the second measure of the bond properties according to AIM, is barely below zero, and remains ca. −0.02 in the B conformer and −0.013 au in the A conformer, which could indicate weak hydrogen-bonding regions. However, for the IHBs found in this work, the Laplacian at the bond critical point tends to be negative (although small), and smaller than that for an intermolecular hydrogen bond, suggesting that the threshold for this descriptor should be revised. This analysis indicates that the main influence on the stability of the B conformer is the IHB between the two moieties of the molecule.

NMR chemical shifts

The experimental ^{13}C NMR chemical shifts of clindamycin fall within the interval 16–90 pm [11]. The B3LYP/aug-pcS-1 values are shown in Table 5. The calculated values for the ^{13}C chemical shifts are in fairly good agreement with the experimental data. As chemical shifts are sensitive to subtle changes in the electronic structure, which depends in a rather complex manner on the molecular structure, we will now discuss the dependence of the calculated NMR chemical shifts on the conformation and the IHB. As usual, the central part of the molecule is the most interesting part to consider for this purpose. The chemical shifts of the carbon atoms are predicted to be located in their usual ranges: δ(^{13}C=O) near to 185 ppm, δ(^{13}C–H) close to 70 ppm. δ(^{13}C=O) exhibits a sensitivity to IHB: the highest value (188.6 ppm) occurs for the B conformer of clindamycin, which is stabilized by the C19–O9···H37–O6 intramolecular hydrogen bond more than the A conformer (185.1 ppm) is stabilized by the C19–O9···H37–O6 bond. The δ(^{15}N) chemical shifts vary from −350 to ca. −280 ppm. These chemical shifts have also been shown to depend strongly on the local properties of the electron density. The small absolute value of the chemical shift of N2 in the B conformer is in line with the small absolute value of the charge density on this nucleus (−0.547 in the A conformer and −0.530 in the B conformer). Finally, it is clear that δ(^{17}O) can be classified into two groups. In the first group, the oxygen acts as the roton acceptor for the OH group, and its chemical shift is lower for the B conformer than for the A conformer of clindamycin. The chemical shift of the hydroxyl oxygen O6 is the highest for the A conformer (considering its absolute value), and the same is true of the oxygen O7 in the ring.

The calculated oxygen chemical shifts correlate with the charges, but they are of limited diagnostic value due to the large line widths in the oxygen NMR spectra.

Finally, let us now focus on the conformational sensitivities of individual spin–spin coupling constants (SSCC). The selected intramolecular SSCCs are gathered in Fig. 8. Some coupling constants vary with changes in

Table 5 B3LYP/aug-pcS-1 calculated chemical shifts for both clindamycin "exp-opt" conformers optimized at the B3LYP/6-31G** level in vacuum. We used ^{1}H (TMS)=31.50, ^{13}C (TMS)=182.20, ^{15}N (CH_3NO_2)=167.89, ^{17}O (CH_3NO_2)=−389.95 (+605), ^{33}S (CS_2)=1131.94, and ^{35}Cl (NaCl)=151.02 as references

Atom	Chemical shifts (ppm)		Experimental value [11]
	A	B	
S1	−350.15	−342.59	–
N2	−293.38	−285.97	–
N3	−347.65	−349.95	–
O4	63.47	51.98	–
O5	72.56	65.78	–
O6	85.97	72.67	–
O7	34.21	32.74	–
O9	295.05	260.14	–
C10	19.7	20.9	15.5
C11	98.74	104.44	90.0
C12	77.66	79.92	70.5
C13	76.95	77.63	73.2
C14	73.11	76.87	70.9
C15	72.95	78.14	71.8
C16	65.72	62.1	55.8
C17	71.13	77.03	60.7
C18	25.17	26.44	24.5
C19	185.06	188.59	172.4
C20	78.9	78.62	71.1
C21	43.24	43.48	43.4
C22	71.04	70.74	64.3
C23	43.05	46.37	39.3
C24	41.47	44.96	38.7
C25	43.59	44.53	37.0
C26	27.96	29.75	23.3
C27	17.6	18.89	16.0
Cl28	341.29	336.87	–

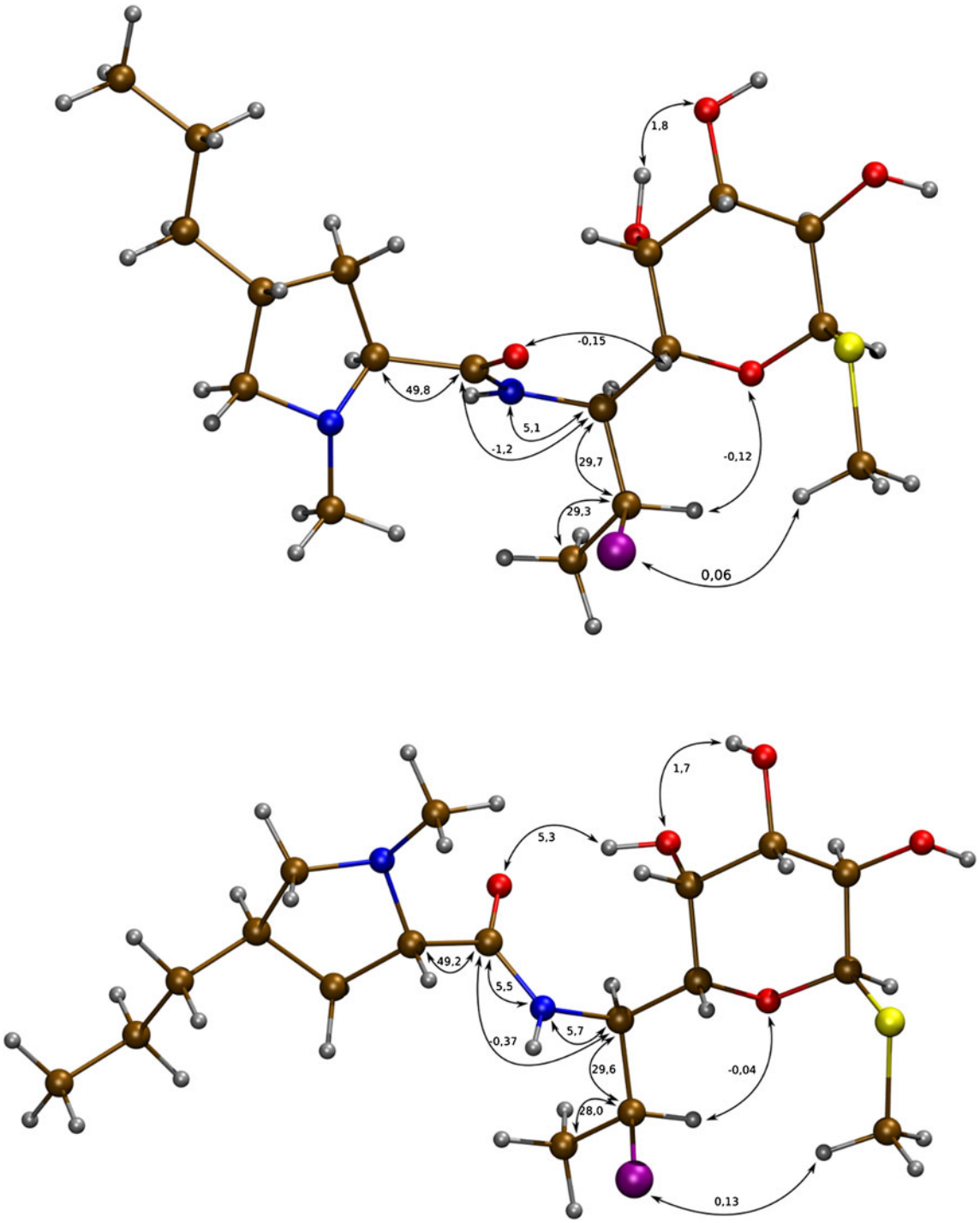

Fig. 8 The selected B3LYP/aug-pcJ-0 calculated spin–spin constants *J* (in Hz) for both "exp-opt" conformers of clindamycin, i.e., A (*top*) and B (*bottom*), optimized at the B3LYP/6-31G** level in vacuum

conformation; for example $^{1}J_{C15–C16}$ changes from 5.1 to 5.7 Hz when moving from the A to the B conformer. However, more interesting is the $^{1}J_{H37–O9}$ SSCC transmitted through the C=O···H–O IHB, which is equal to 5.3 Hz in the B conformer. This value is large enough to be measured experimentally.

Conclusions

We have quantum chemically characterized the two conformers of each of the known lincosamides clindamycin, lincomycin, and pirlimycin at the B3LYP/6-31G** level. Internal rotations in clindamycin were investigated in vacuum

and within the framework of the IEF-PCM model [21]. Using NBO analysis, and with the aid of the AIM theory, we have characterized the intramolecular hydrogen bonds in these molecules. We focused on the sensitivities of electronic structure parameters such as NBO atomic charges, bond critical points, NMR chemical shifts, and spin–spin coupling constants to the conformation of clindamycin.

The two most stable conformers of clindamycin exhibit C=O···H–O intramolecular hydrogen bonds. According to NBO and AIM analyses, the presence of this internal hydrogen bond between the pyrrolidine-derivative ring and the six-atom sugar (methylthiolincosamide) is the main influence on conformer stability in vacuum and in water.

Acknowledgements We acknowledge support from University of Warsaw (ICM/BST, G31-4 and G18-4), the Polish Ministry of Science and Higher Education (N N301 245236), and the Foundation for Polish Science. JT is supported by the Team project (TEAM/2009-3/8), which is co-financed by European Regional Development Fund and operates within the Innovative Economy Operational Programme. KKM is supported by the EU through the European Social Fund (contract no. UDA-POKL.04.01.01-00-072/09-00).

References

1. Liljas A. (2004) Structural aspects of protein synthesis. World Scientific, Singapore
2. Tenson T, Lovmar M, Ehrenberg M (2003) J Mol Biol 330 (5):1005–1014
3. Spizek J, Rezanka T (2004) Appl Microbiol Biotechnol 64:455–464
4. Lion C, Escande F, Burdin J (1996) Eur J Epidemiol 12(5):521–533
5. Nir-Paz R, Block C, Shasha D, Korenman Z, Gorodnitzky Z, Jaffe J, Ron M, Michael-Gayego A, Cohen-Poradosu R, Shapiro M, Moses A (2006) Int J Antimicrob Agents 28(4):313–319
6. Kehrenberg C, Schwarz S, Jacobsen L, Hansen L, Vester B (2005) Mol Microbiol 57(4):1064–1073
7. Poehlsgaard J, Pfister P, Bottger E, Douthwaite S (2005) Antimicrob Agents Chemother 49(4):1553–1555
8. Roberts M, Sutcliffe J, Courvalin P, Jensen L, Rood J, Seppala H (1999) Antimicrob Agents Chemother 43(12):2823–2830
9. Ravikumar K, Sridhar B (2010) Acta Crystallogr C 66:97–100
10. Rajeswaran M, Srikrishnan T (2004) Carbohydr Res 339 (12):2111–2115
11. Verdier L, Bertho G, Gharbi-Benarous J, Girault J (2000) Bioorg Med Chem 8:1225–1243
12. Morar M, Bhullar K, Hughes D, Junop M, Wright G (2009) Structure 17(12):1649–1659
13. Schlünzen F, Zarivach R, Harms J, Bashan A, Tocilj A, Albrecht R, Yonath A, Franceschi F (2001) Nature 413:814–821
14. Tu D, Blaha G, Moore P, Steitz T (2005) Cell 121(2):257–270
15. Dunkle J, Xiong L, Mankin A, Cate J (2010) Proc Natl Acad Sci USA 107:17152–17157
16. Harms J, Wilson D, Schluenzen F, Connell S, Stachelhaus T, Zaborowska Z, Spahn C, Fucini P (2008) Mol Cell 30(1):26–38
17. Berman H, Westbrook J, Feng Z, Gilliland G, Bhat TN, Weissig H, Shindyalov IN, Bourne P (2000) Nucleic Acids Res 28:235–242
18. Becke A (1993) J Chem Phys 98:5648–5652
19. Lee C, Yang W, Parr R (1988) Phys Rev B 37:785–789
20. Peng C, Ayala P, Schlegel H, Frisch M (1996) J Comp Chem 17:49–56
21. Tomasi J, Mennucci B, Cammi R (2005) Chem Rev 105(8):2999–3093
22. Hall G, Smith C (1984) Int J Quantum Chem 25:881–890
23. Smith C, Hall G (1986) Theor Chem Acc 69:63–69
24. Schuler L, Daura X, van Gunsteren W (1996) J Comp Chem 22 (11):1205–1218
25. Jensen F (2008) J Chem Theory Comp 4:719–725
26. London F (1937) J Phys Radium 8:397–409
27. McWeeny R (1962) Phys Rev 126:1028
28. Ditchfield R (1974) Mol Phys 27:789–807
29. Wolinski K, Hilton J, Pulay P (1990) J Am Chem Soc 112:8251–8260
30. Cheeseman J, Trucks G, Keith T, Frisch M (1996) J Chem Phys 104:5497–5509
31. Jensen F (2006) J Chem Theory Comp 2:1360–1369
32. Jensen F (2010) Theor Chem Acc 126:371–382
33. Feller D (1996) J Comp Chem 17(13):1571–1586
34. Schuchardt K, Didier B, Elsethagen T, Sun L, Gurumoorthi V, Chase J, Li J, Windus T (2007) J Chem Inf Model 47(3):1045–1052
35. Frisch M et al. (2004) Gaussian 03, revision C.02. Gaussian, Inc., Wallingford
36. Weinhold F, Landis C (2001) Chem Educ Res Pract 2:91–104
37. Biegler-önig F, Schönbohm J, Bayles D (2001) J Comp Chem 22:545–559
38. Allouche A (2011) J Comp Chem 32:174–182
39. Humphrey W, Dalke A, Schulten K (1996) J Molec Graph 14:33–38
40. Arunan E, Desiraju G, Klein R, Sadlej J, Scheiner S, Alkorta I, Clary D, Crabtree R, Dannenberg J, Hobza P, Kjaergaard H, Legon A, Mennucci B, Nesbitt D (2011) Pure Appl Chem 83 (8):1619–1636
41. Arunan E, Desiraju G, Klein R, Sadlej J, Scheiner S, Alkorta I, Clary D, Crabtree R, Dannenberg J, Hobza P, Kjaergaard H, Legon A, Mennucci B, Nesbitt D (2011) Pure Appl Chem 83(8):1637–1641
42. Reed A, Curtiss L, Weinhold F (1988) Chem Rev 88:899–926
43. Poater J, Solá M, Bickelhaup F (2006) Chem Eur 12:2889–2901
44. Popelier P (2000) Atoms in Molecules. An introduction. Prentice Hall, Harlow
45. Matta C, Boyd RBA (eds)(2007) The quantum theory of atoms in molecules: from solid state to DNA and drug design. Wiley-VCH, Weinheim
46. Koch U, Popelier P (1995) J Phys Chem 99(24):9747–9754
47. Woodford J (2007) J Phys Chem A 111:8519–8530